Article

Stabilization of Cu/Ni Alloy Nanoparticles with Graphdiyne Enabling Efficient CO_2 Reduction

FU Xinliang[1], ZHU Aonan[1], CHEN Xiaojie[1], ZHANG Shifu[2], WANG Mei[2]✉ and YUAN Mingjian[1]✉

Received August 29, 2021
Accepted September 30, 2021

Electrocatalysis has become an attractive strategy for the artificial reduction of CO_2 to high-value chemicals. However, the design and development of highly selective and stable non-noble metal electrocatalysts that convert CO_2 to CO are still a challenge. As a new type of two-dimensional carbon material, graphdiyne(GDY), is rarely used to explore the application in carbon dioxide reduction reaction(CO_2RR). Therefore, we tried to use GDY as a substrate to stabilize the copper-nickel alloy nanoparticles(NPs) to synthesize Cu/Ni@GDY. Cu/Ni@GDY requires an overpotential (–0.61 V) to 10 mA/cm^2 for the formation of CO, and it shows better activity than Au and Ag, achieving a higher Faraday efficiency of about 95.2% and high stability of about 26 h at an overpotential (–0.70 V). The electronic interaction between GDY substrate and Cu/Ni alloy NPs and the large specific surface area of GDY is responsible for the high performance.

Keywords Graphdiyne(GDY); Carbon dioxide reduction reaction (CO_2RR); CO; Electrocatalysis; Cu/Ni alloy nanoparticle

1 Introduction

In order to meet the ever-increasing energy demand and environmental problems, reducing carbon dioxide to fossil fuels is one of the most promising solutions. However, carbon dioxide is a linear molecule that is completely oxidized and extremely stable. It requires an efficient and stable catalyst to realize the slow kinetic reduction process. In the past few decades, a large number of carbon dioxide catalysts have been designed, and precious metals, such as Ag and Au are still relatively excellent catalysts[1,2]. However, their low natural abundance and relatively high cost make it difficult to achieve large-scale applications. Copper-based catalysts are still unique catalysts that can produce both C_1 and multi-carbon products in electrocatalytic reduction. Its copper-based catalysts related to molecular complexes, alloys, oxides, nanoparticles(NPs), and flake structures appear at the forefront of carbon dioxide reduction reaction(CO_2RR)[3—6]. Despite the poor selectivity of copper-based catalysts, the catalytic activity and selectivity of copper nanoparticles can be controlled by the "size effect" and alloying, making them the most promising candidate for high-efficiency electrocatalysts, and have caused widespread concern due to their strong controllability[7,8]. However, high surface energy small-sized nanoparticles usually undergo severe self-aggregation during the electrocatalytic reaction process, which leads to the degradation or deactivation of the active sites of the catalyst, and ultimately leads to a decrease in the catalytic performance of the catalyst. Therefore, there is an urgent need to stabilize ultra-small nanoparticles to maximize the utilization and long-term stability of the catalyst's efficiency. However, solutions dedicated to solving this problem are still rarely explored and still a challenge.

The main obstacle to overcoming the aggregation of nanoparticles is how to balance the surface energy of ultra-small nanoparticles. Several spatially-confined methods and ligand-assisted growth have been explored. Space traps are prepared by preparing support materials with special morphologies or encapsulating metal particles in special structures[9—11]. Although these methods solved the problem of cluster self-aggregation to a certain extent, they are difficult to achieve large-scale applications due to their complex preparation processes. In addition, ligand-assisted growth can also achieve the synthesis of ultra-small nanoparticles, but a large number of ligands are required to stabilize the structure and a large number of ligands will sacrifice the conductivity of the catalyst[12]. Therefore, finding a suitable and effective catalyst support material, which not only improves the dispersity of the catalyst and stabilizes nanoparticles, but also can promote mass transfer, is a possible solution to this problem.

Graphdiyne(GDY) is a new type of carbon allotrope, composed of *sp*(—C≡C—) and *sp*^{2} hybrid materials, in which two acetylene bonds are connected to the benzene ring. Due to its periodic large π-conjugation, large specific surface area, natural uniformly distributed pore structure, excellent thermal and chemical stability, and outstanding electrical conductivity, the intrinsic charge carrier mobility of GDY is higher than that

✉ YUAN Mingjian
yuanmj@nankai.edu.cn
✉ WANG Mei
meiwang@ouc.edu.cn
1. Key Laboratory of Advanced Energy Materials Chemistry, Ministry of Education, Renewable Energy Conversion and Storage Center(RECAST), College of Chemistry, Nankai University, Tianjin 300071, P. R. China;
2. Key Laboratory of Marine Chemistry Theory and Technology, Ministry of Education, College of Chemistry and Chemical Engineering, Ocean University of China, Qingdao 266100, P. R. China

https://doi.org/10.1007/s40242-021-1344-7

of graphene. GDY has shown great application prospects in the fields of hydrogen evolution reaction(HER), oxygen evolution reaction(OER), water-splitting, reduction of nitrogen, and lithium batteries[13—18]. GDY with abundant acetylene bonds can adsorb metal ions, stabilize metal particles, and provide an opportunity for charge transfer between the GDY substrate and metal nanoparticles, which are conducive to the improvement of catalyst performance. In addition, its unique porous structure has strong adsorption energy for metal nanoparticles, which can reduce the surface energy of metal nanoparticles and be beneficial for stabilizing metal particles. Inspired by the above ideas, we designed Cu/Ni@GDY for CO_2RR. Cu/Ni alloy nanoparticles are prepared by the solution method. Cu/Ni alloy nanoparticles loaded to GDY are achieved through ligand exchange and assisted precipitation. The prepared Cu/Ni@GDY shows highly efficient and selective electroreduction of CO_2 to CO, with a Faraday efficiency(FE) as high as 95.2%, which is comparable to the noble metal catalysts, such as gold and silver, and exhibits ultra-long stability. During the 26-h electrolysis process, the current density and Faraday efficiency remained relatively stable. This enriches the catalyst support system for stabilizing nanoparticles, provides a universal method, and can be extended to the catalytic applications of other catalysts.

2 Experimental

2.1 Reagents

Reagents were purchased from commercial vendors and used as received. The solvent is reagent grade or higher purity. All manipulations were conducted in Ar unless otherwise specified. Cu sheet(thickness: 1.6 mm, Shanghai Guoyao Chemicals Co., Ltd.) was used as received. Deionized water (resistivity: 18.3 MΩ·cm) was used for the preparation of all aqueous solutions.

2.2 Synthesis of Cu/Ni Alloy Nanoparticles

CuNi alloy nanoparticles were synthesized as previously reported[19]. First, 65 mg of $Cu(acac)_2$ and 10 mg of $Ni(acac)_2$ were dissolved in a mixture of 12.5 mL of diphenyl ether, 8.5 mL of oleylamine, and 1.7 mL of oleic acid. The solution was placed in an oil bath, heated at 240 °C for around 10 min, and 100 mg of borane morpholine complex was added. The temperature was kept at 240 °C for another 40 min. After the solution was cooled to room temperature, the product was precipitated with ethanol and then centrifuged(9000 r/min, 10 min). This step was repeated twice by using ethanol, and the resulting nanoparticles were collected by dispersing them in hexane. For the synthesis of copper-nickel alloys with different ratios, the ratio of copper acetylacetonate and nickel acetylacetonate needs to be changed. The composition of the obtained nanoparticles was determined by the inductively coupled plasma optical emission spectrameter(ICP-OES) analysis.

2.3 Synthesis of Cu/Ni@GDY

The prepared GDY and Cu/Ni alloy nanoparticles were dispersed into 50 mL of *n*-hexane and sonicated for 30 min. Slowly adding DMF gradient to wash away the ligand several times and Cu/Ni@GDY was obtained by co-precipitation, which is annealed in Ar atmosphere to remove the remaining ligand at 230 °C.

2.4 Preparation of GDY/CP Electrode

First, 5 mg of GDY, Cu/Ni, or Cu/Ni@GDY powders were dispersed into a mixed solution containing Nafion(20%, 5 μL) and ethanol(950 μL). Then 100 μL of the mixed solution was dropped on the carbon paper and the catalyst loading is about 0.5 mg/cm^2.

2.5 Physical Characterization

The surface morphology of the sample was measured on a high-resolution transmission electron microscope(HRTEM FEI Talos F200×G2) and a field emission scanning electron microscope(SEM JEOL JSM-7500F). Raman spectrum was measured under 532 nm laser excitation(Laser Confocal Raman, LabRAM HR-Evolution). Quantitative element analysis was *via* ICP-OES(SpectroBlue- IL). X-Ray powder diffraction(XRD, D/max-2500), X-ray photoelectron spectroscopy(XPS Thermo Scientific ESCALAB 250Xi), and XPS measurements were calibrated to the C_{1s}(284.8 eV). Gas-phase product is detected by the home-built gas chromatography (GC-2014C，Shimadzu).

2.6 Electrochemical Characterization

CHI-760E electrochemical workstation was used for all electrochemical measurements in a typical three-electrode system and the pre-treatment sample was the working electrode; platinum sheet and Ag/AgCl correspond to the counter electrode and the reference electrode, respectively. The CO_2RR tests were carried out in 0.1 mol/L $KHCO_3$ solution with a sweep rate of 5 mV/s. Cyclic voltammetry(CV) was performed in a non-faradaic region of the voltammogram with different scan rates. Electrochemical impedance spectroscopy (EIS) measurements of the catalysts were performed at open

https://doi.org/10.1007/s40242-021-1344-7

voltage with the frequency range from 100 kHz to 10 MHz. The long-time stability tests for samples were performed using chronopotentiometry at a constant applied voltage. The equivalent circuit simulation diagram is simulated by Zview with reference to the reported literature[11].

3 Results and Discussion

3.1 Morphological Characterization

The bulk GDY was synthesized with a bottom-up *in situ* Glaser-Hay cross-coupling reaction method from 1,2,3,4,5,6-hexakis((trimethylsilyl)ethynyl)benzene(Scheme S1, see the Electronic Supplementary Material of this paper)[20]. The scanning electron microscopy(SEM) image displays uniform and flakes of GDY(Fig.S1, see the Electronic Supplementary Material of this paper). As shown in Fig.1(A) and (B), TEM images reveal that the films are two-dimensional planar stacked materials with a certain roughness. The unique two-dimensional planar structure makes GDY have a larger specific surface area, which will facilitate the adsorption of nanoparticles and mass transfer in the electrolyte. Then the Cu/Ni@GDY is prepared by co-precipitation, where the solution contains Cu/Ni alloy nanoparticles[Fig.1(C)] of uniform size and GDY. As shown in Fig.1(D), copper-nickel alloy nanoparticles are uniformly distributed on the graphyne surface with average diameters below 5 nm and no obvious aggregation is observed(Figs.S2—S4, see the Electronic Supplementary Material of this paper). The element analysis of the catalyst reveals the uniform distribution of elements Cu and Ni on the surface of the GDY film. The above results clearly prove that Cu/Ni alloy nanoparticles loaded on GDY are successfully synthesized, and also show that GDY can anchor ultra-small nanoparticles.

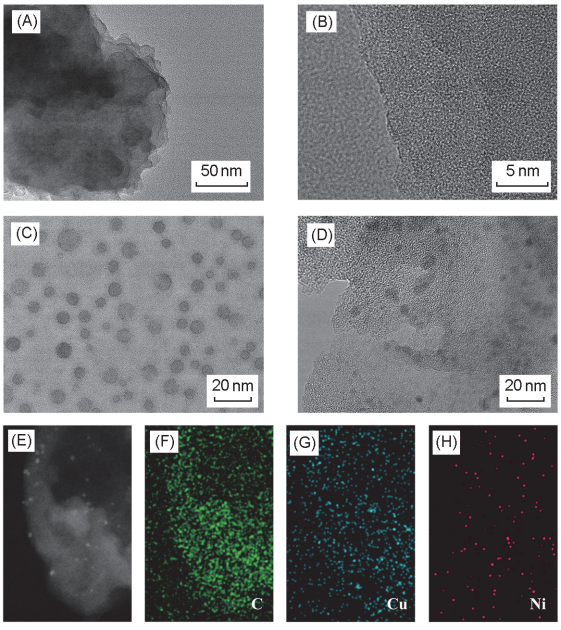

Fig.1 TEM(A) and HRTEM(B) images of GDY, HRTEM image of Cu/Ni alloy nanoparticles(C), HRTEM image of Cu/Ni@GDY(D), and EDS element mappings of Cu/Ni@GDY: (E) HAADF-STEM, (F) C, (G) Cu, (H) Ni

3.2 Structure and Composition Characterization

The structure of the catalyst was further characterized by XRD, Raman, and XPS. Fig.2(A) displayed XRD patterns, in Fig.2(A), the main peaks of Cu/Ni@GDY and Cu/Ni are attributed to the peak of Cu, and the Cu peak of Cu/Ni moves to a high degree relative to the JCPDS No. 04-0836 of Cu. This may be attributed to the distortion of the crystal lattice caused by the stress of the phase interface between the two metals. Ni is not observed in the XRD pattern, which may be due to its low content and is consistent with the composition confirmed by ICP-OES ($Cu_{95}Ni_5$). Fig.2(B) shows the shape of the classic peak of GDY, two strong peaks of D and G bands at 1386 and 1576 cm^{-1} for GDY, which is attributed to E_{2g} stretching vibrations in the aromatic ring of sp^2-hybridized, and defects of structure and degree of disorder. The weaker peak is around 1931 cm^{-1}, indicating the presence of terminal alkynyl groups in GDY. Another weak peak is at 2185 or 2164 cm^{-1} for GDY or Cu/Ni@GDY, which attributed to the vibration of diyne linkages. A weak peak at around 2200 cm^{-1} for diyne linkages and a broad peak at 22.5 degrees were also confirmed by FTIR and XRD patterns(Figs.S5 and S6, see the Electronic Supplementary Material of this paper). Therefore, we have now confirmed that copper-nickel alloy nanoparticles have been successfully loaded onto GDY. Compared with traditional GDY, the characteristic vibration peak of the

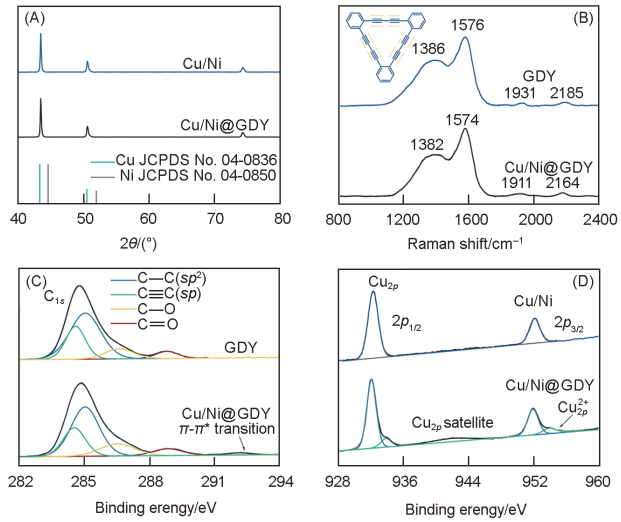

Fig.2 XRD pattern of Cu/Ni alloy nanoparticles and Cu/Ni@GDY(A), Raman spectroscopy of GDY and Cu/Ni@GDY(B), high-resolution XPS spectrum of C_{1s} for GDY and Cu/Ni@GDY(C), and high-resolution XPS spectra of Cu_{2p} for Cu/Ni alloy nanoparticles and Cu/Ni@GDY(D)

https://doi.org/10.1007/s40242-021-1344-7

acetylene bond shifts to a low wavenumber obviously after the GDY is loaded with copper-nickel alloy nanoparticles, which indicates that there is a strong electronic interaction between the GDY and the Cu/Ni alloy nanoparticles[21].

The chemical composition and chemical state of the sample are also revealed using X-ray photoelectron spectroscopy(XPS). The survey scan result of XPS unambiguously demonstrates that Cu/Ni@GDY contains C, Cu, Ni, and O, and GDY is only composed of C and O, which is consistent with the elemental analysis of TEM(Figs.S7 and S8, see the Electronic Supplementary Material of this paper). In detail, the peaks of C_{1s} in GDY can be divided into four peaks, including sp^2 and sp at binding energies of 284.6 and 285.1 eV, C—O at 286.8 eV, and C═O at 288.8 eV, which have been assigned to a C_{1s} orbital of C—C(sp^2), C—C(sp), C—O and C═O, respectively, in Fig.2(C). A new peak was observed in the C_{1s} orbital of Cu/Ni@GDY at 291.6 eV, which is a π-π^* transition peak and consistent with the literature report[21]. Therefore, we can conclude that there is an electronic interaction between GDY and Cu/Ni nanoparticles, which also validates the results of Raman spectroscopy. The copper 2p high-resolution spectrum of Cu/Ni@GDY is shown in Fig.2(D) and the two main peaks are $Cu_{2P_{1/2}}$(932.7 eV) and $Cu_{2P_{3/2}}$(952.5 eV). The shoulder peak near the main peak is attributed to the Cu^{2+}, which indicates that the copper on the surface of the Cu/Ni nanoparticle will be part of the oxygen ring during the process of removing the ligand and loading it on the GDY. In addition, the copper 2p orbital of Cu/Ni@GDY moves to a lower binding energy compared with Cu/Ni, which implies that charge transfer occurs between GDY and Cu/Ni nanoparticles, and the same trend is also observed in the peaks of $Ni_{2p_{3/2}}$ and $Ni_{2p_{1/2}}$(Figs.S10 and S11, see the Electronic Supplementary Material of this paper)[22]. The above results prove that the Cu/Ni alloy nanoparticles can be loaded on GDY, and can maintain excellent dispersity and stability, and electronic interaction exists between GDY and Cu/Ni nanoparticles. In addition, there is a strong electronic interaction between the GDY substrate and the Cu/Ni alloy nanoparticles, which is beneficial to facilitate the charge transfer process of the electrocatalytic reaction.

3.3 CO_2RR Performance and Stability of the Catalyst

The electrocatalyst CO_2RR activity of Cu/Ni@GDY was evaluated in a CO_2-saturated 0.1 mol/L $KHCO_3$ solution in an H-type cell. As shown in Fig.3(A), GDY has almost no catalytic activity. Compared with the polarization curves of GDY and Cu/Ni, the Cu/Ni@ GDY shows a rapid response to the applied potential, and the current increases rapidly at a more negative potential, which can be attributed to the significant increase in CO_2RR activity. When the applied voltage reaches 0.61 V, the current density of Cu/Ni@ GDY reaches 10 mA/cm^2. Under the same conditions, the current density of Cu/Ni@GDY is about 3 times that of Cu/Ni and 100 times that of GDY(Fig.S12, see the Electronic Supplementary Material of this paper). In the constant voltage catalytic electrochemical reduction of CO_2,

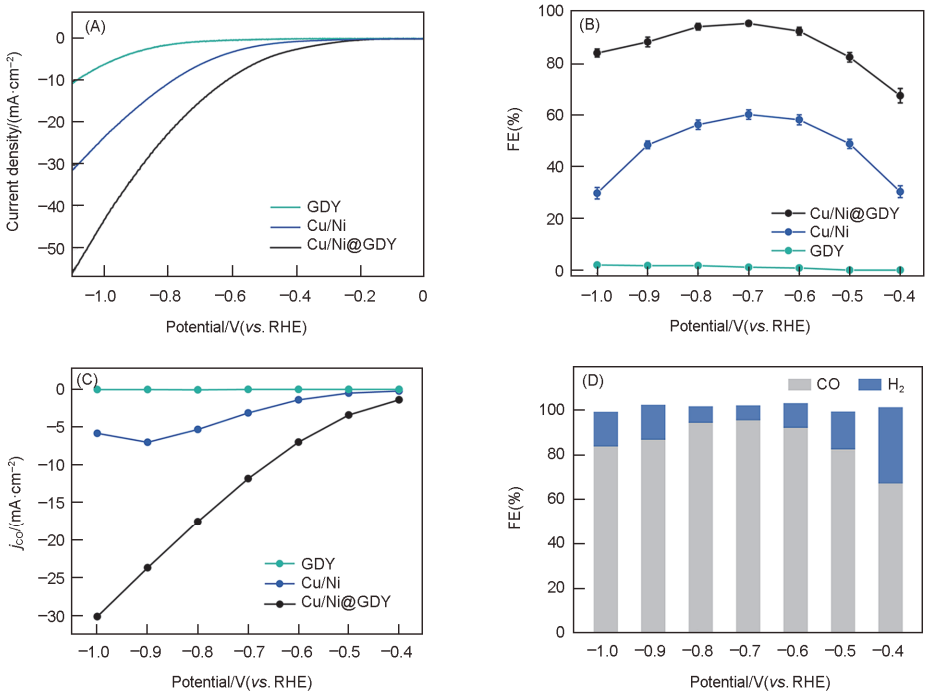

Fig.3 Linear sweep voltammetry(LSV) of GDY, Cu/Ni, and Cu/Ni@GDY(A), FE_{CO} of GDY, Cu/Ni and Cu/Ni@GDY(B) and corresponding j_{CO} of GDY, Cu/Ni and Cu/Ni@GDY(C), and FE toward CO and H_2 of Cu/Ni@GDY(D)

https://doi.org/10.1007/s40242-021-1344-7

two gas-phase products of CO and hydrogen are detected. As shown in Fig.3(B), the Faraday efficiency(FE) of the Cu/Ni@GDY sample increases first and then decreases as the applied voltage increases, reaching the highest conversion efficiency of 95.2% at 0.7 V. Compared with GDY and Cu/Ni, the Cu/Ni@ GDY has a wider work voltage window[Fig.3(D), and Figs.S13 and S14, see the Electronic Supplementary Material of this paper]. The maximum value of the CO current density(j_{CO}) of Cu/Ni@ GDY is 37 mA/cm^2, which is about 6 times higher than that of the comparison catalyst. High FE and a larger partial current density show that the CO_2RR activity of Cu/Ni@ GDY is better than those of GDY and Cu/Ni. Then a long-term constant voltage test was used to evaluate the stability of the catalyst, and samples were taken every 1 h to detect the FE of the product recorded by gas chromatography. As shown in Fig.4(A), the Cu/Ni@ GDY current density remained relatively stable during the continuous electrolysis process for up to 26 h. On the contrary, the stability of Cu/Ni dropped sharply in the first few hours. FE_{CO} of Cu/Ni@GDY also remains relatively stable and exceeds 90% after 26 h of testing[Fig.4(B)]. The above results fully prove that Cu/Ni@ GDY has excellent stability, which is due to the stability of GDY's chemical structure and alloy nanoparticles stabilized by GDY.

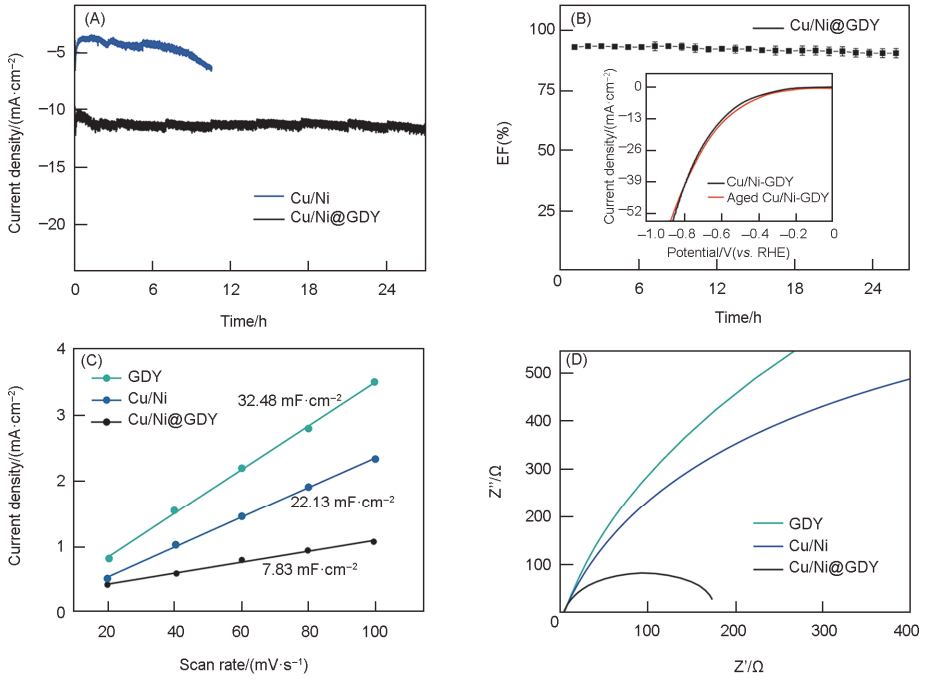

Fig.4 Stability and the origination of performance catalysts

(A) Stability testing at −0.70 V for Cu/Ni@GDY; (B) corresponding FEco. Insert: change of LSV after stability test; (C) capacitive currents as a function of scan rates; (D) electrochemical impedance spectroscopy of GDY, Cu/Ni, and Cu/Ni@GDY.

3.4 Discussion on the Reasons for the High Performance of the Catalyst

In order to explore the origination that the Cu/Ni@GDY catalyst has excellent catalytic performance, we calculated the electric double-layer capacitance of the catalyst by cyclic voltammetry to further obtain the electrochemical surface area(ECSA), which is an important factor affecting the catalytic performance(Figs.S15—S17, see the Electronic Supplementary Material of this paper). From Fig.4(C), the ECSA of Cu/Ni@GDY is approximately 1.5 times that of Cu/N-C and 4 times that of GDY. A larger ECSA can provide more catalytically active sites, which is one of the necessary conditions for high-performance catalysts. The unique two-dimensional planar structure of GDY has a larger specific surface area, which provides a larger specific surface area to adsorb Cu/Ni nanoparticles, which also confirms that the Cu/Ni@GDY has a higher ECSA. In addition, we use Tafel slope and electrochemical impedance spectroscopy(EIS) to study the charge transfer of the catalytic process. A smaller Tafel slope indicates better catalytic activity in general, and by comparing with the two ideal Tafel slopes obtained from the empirical equation, the decisive step in the process of catalytic reaction can be preliminarily obtained. For example, the Tafel slope of 118 mV/dec means that the rate-determining step of CO_2RR is the initial single electron transfer step to generate intermediate $*CO_2^-$, which is the key intermediate[23]. The Tafel slope of Cu/Ni@GDY is close to the theoretical value of 118 mV/dec, which means that the transfer of single electrons to CO_2 to form intermediate $*CO_2^-$ is the rate-determining step of the reaction. Compared with Cu/Ni and GDY, the smaller

https://doi.org/10.1007/s40242-021-1344-7

Tafel slope of Cu/Ni@GDY represents faster charge transfer, which indicates that the catalyst has certain advantages in the kinetics of CO formation during the catalytic reaction process(Fig.S18, see the Electronic Supplementary Material of this paper). Electrochemical impedance spectroscopy(EIS) was also used to further explain the reaction kinetics of the CO_2RR. As shown in Fig.4(D), compared with the other two samples, the charge transfer resistance of Cu/Ni@GDY is significantly reduced, indicating that it has an ideal electron transfer process and fast catalytic kinetics. In the fitted circuit diagram(Fig.S19, see the Electronic Supplementary Material of this paper), R_s stands for the solution resistance, Q is related to the electric double-layer capacitance, and R stands for the charge transfer resistance. According to the simulation results, the Cu/Ni@GDY electrode has the smallest charge transfer resistance, which is conducive to the improvement of charge transfer and catalytic performance. Faster charge transfer in the CO_2RR process can greatly improve catalytic efficiency. This is due to the electronic interaction between GDY and Cu/Ni nanoparticles.

4 Conclusions

In summary, the novel CO_2RR catalyst Cu/Ni@GDY can be prepared by a simple solution method. Graphdiyne in the composite catalyst can not only promote charge transfer but also stabilize nanoparticles, due to the strong electronic interaction between graphyne and metal nanoparticles. Cu/Ni@GDY is proven as an electrocatalyst for highly efficient and selective electroreduction of CO_2 to CO. In 0.1 mol/L $KHCO_3$, this catalyst achieves a high FE_{CO} of 95.2% at –0.7 V with ultra-long electrochemical stability. This strategy may open an avenue for GDY-based catalysts to stabilize nanoparticles and pave the way for the development of stable and efficient CO_2RR catalysts in the near future.

Electronic Supplementary Material

Supplementary material is available in the online version of this article at http://dx.doi.org/10.1007/s40242-021-1344-7.

Acknowledgements

This work was supported by the National Natural Science Foundation of China (Nos.21771114, 91956130) and the Distinguished Young Scholars of Tianjin, China(No.19JCJQJC62000).

Conflicts of Interest

The authors declare no conflicts of interest.

References

[1] Ringe S., Morales-Guio C. G., Chen L. D., Fields M., Jaramillo T. F., Hahn C., Chan K., *Nat. Commun.,* **2020**, *11*(1), 33
[2] Bhargava S. S., Proietto F., Azmoodeh D., Cofell E. R., Henckel D. A., Verma S., Brooks C. J., Gewirth A. A., Kenis P. J. A., *Chem ElectroChem,* **2020**, *7* (9), 2001
[3] De Gregorio G. L., Burdyny T., Loiudice A., Iyengar P., Smith W. A., Buonsanti R., *ACS Catal.,* **2020**, *10*(9), 4854
[4] Li H., Liu T., Wei P., Lin L., Gao D., Wang G., Bao X., *Angew Chem. Int. Ed. Engl.,* **2021**, *60*(26), 14329
[5] Zhang B., Zhang J., Hua M., Wan Q., Su Z., Tan X., Liu L., Zhang F., Chen G., Tan D., Cheng X., Han B., Zheng L., Mo G., *J. Am. Chem. Soc.,* **2020**, *142*(31), 13606
[6] Li F., Thevenon A., Rosas-Hernandez A., Wang Z., Li Y., Gabardo C. M., Ozden A., Dinh C. T., Li J., Wang Y., Edwards J. P., Xu Y., McCallum C., Tao L., Liang Z. Q., Luo M., Wang X., Li H., O'Brien C. P., Tan C. S., Nam D. H., Quintero-Bermudez R., Zhuang T. T., Li Y. C., Han Z., Britt R. D., Sinton D., Agapie T., Peters J. C., Sargent E. H., *Nature,* **2020**, *577*(7791), 509
[7] Huang J., Mensi M., Oveisi E., Mantella V., Buonsanti R., *J. Am. Chem. Soc.,* **2019**, *141*(6), 2490
[8] Rong W., Zou H., Zang W., Xi S., Wei S., Long B., Hu J., Ji Y., Duan L., *Angew. Chem. Int. Ed. Engl.,* **2021**, *60*(1), 466
[9] Wang Z. L., Sun K., Henzie J., Hao X., Li C., Takei T., Kang Y. M., Yamauchi Y., *Angew. Chem. Int. Ed. Engl.*, **2018**, *57*(20), 5848
[10] Wang C., Guan E., Wang L., Chu X., Wu Z., Zhang J., Yang Z., Jiang Y., Zhang L., Meng X., Gates B. C., Xiao F. S., *J. Am. Chem. Soc.,* **2019**, *141*(21), 8482
[11] Li X., Yu J., Jia J., Wang A., Zhao L., Xiong T., Liu H., Zhou W., *Nano Energy,* **2019**, *62*, 127
[12] Liu M., Liu M., Wang X., Kozlov S. M., Cao Z., de Luna P., Li H., Qiu X., Liu K., Hu J., Jia C., Wang P., Zhou H., He J., Zhong M., Lan X., Zhou Y., Wang Z., Li J., Seifitokaldani A., Dinh C. T., Liang H., Zou C., Zhang D., Yang Y., Chan T.-S., Han Y., Cavallo L., Sham T.-K., Hwang B.-J., Sargent E. H., *Joule,* **2019**, *3*(7), 1703
[13] Wang F., Zuo Z., Shang H., Zhao Y., Li Y., *ACS Appl. Mater. Interfaces,* **2019**, *11*(3), 2599
[14] Li J., Gao X., Zhu L., Ghazzal M. N., Zhang J., Tung C.-H., Wu L.-Z., *Energy Environ. Sci.,* **2020**, *13*(5), 1326
[15] Hui L., Xue Y., Yu H., Liu Y., Fang Y., Xing C., Huang B., Li Y., *J. Am. Chem. Soc.,* **2019**, *141*(27), 10677
[16] Li J., Gao X., Liu B., Feng Q., Li X. B., Huang M. Y., Liu Z., Zhang J., Tung C. H., Wu L. Z., *J. Am. Chem. Soc.,* **2016**, *138*(12), 3954
[17] Qi H., Yu P., Wang Y., Han G., Liu H., Yi Y., Li Y., Mao L., *J. Am. Chem. Soc.,* **2015**, *137*(16), 5260
[18] Fang Y., Xue Y., Hui L., Yu H., Liu Y., Xing C., Lu F., He F., Liu H., Li Y., *Nano Energy,* **2019**, *59*, 591
[19] Ma X., Qi K., Wei S., Zhang L., Cui X., *J. Alloys Compd.,* **2019,** *770*, 236
[20] Zhang S., Liu H., Huang C., Cui G., Li Y., *Chem. Commun. (Camb),* **2015**, *51*(10), 1834
[21] Shi G., Xie Y., Du L., Fan Z., Chen X., Fu X., Xie W., Wang M., Yuan M., *Nano Energy,* **2020**, *74*, 104852
[22] Shi G., Fan Z., Du L., Fu X., Dong C., Xie W., Zhao D., Wang M., Yuan M., *Mater. Chem. Front.,* **2019**, *3*(5), 821
[23] Zhu D. D., Liu J. L., Qiao S. Z., *Adv. Mater.,* **2016**, *28*(18), 3423